# A General Framework for Subspace Detection in Unordered Multidimensional Data

Supplementary Material C –
 Voronoi Diagram as Byproduct of the Proposed Subspace
 Detection Framework

Leandro A. F. Fernandes a, Manuel M. Oliveira b

<sup>a</sup>Instituto de Computação, Universidade Federal Fluminense (UFF) CEP 24210-240 Niterói, RJ, Brazil Tel +55 21 2629-5665. Fax +55 21 2629-5669

<sup>b</sup>Instituto de Informática, Universidade Federal do Rio Grande do Sul (UFRGS), CP 15064 CEP 91501-970, Porto Alegre, RS, Brazil

## C.1 Description

This document presents a discussion on how to retrieve an approximation of the dth-order Voronoi diagram [1] of a set of points in  $\mathbb{R}^d$  as byproduct of our subspace detection framework [2]. Such a result is achieved when our approach is applied to the detection of subspaces geometrically interpreted as (d-1)-spheres (e.g., a 0-sphere is a pair of points, a 1-sphere is a circle, a 2-sphere is an ordinary sphere, and so on) in the conformal model of geometry (MOG).

This document also describes how the parameter space of the standard Hough transform (HT) for circle detection from points in the plane is related to the proposed parameter space defined for the same detection case under the conformal MOG.

Email addresses: laffernandes@ic.uff.br (Leandro A. F. Fernandes), oliveira@inf.ufrgs.br (Manuel M. Oliveira).

URLs: http://www.ic.uff.br/~laffernandes (Leandro A. F. Fernandes), http://www.inf.ufrgs.br/~oliveira (Manuel M. Oliveira).

### C.2 Setup of the Proposed Approach

Supplementary Material A shows that the dimensionality of the representational space  $\mathbb{R}^n$  in conformal MOG is n=d+2, where d is the dimensionality of the Euclidean base space, and the two extra dimensions are imposed by the MOG. The first of such extra dimensions is a null vector interpreted as the origin point of the base space (denoted by  $\mathbf{o}$ ), while the second is a null vector interpreted as the point at infinity (denoted by  $\mathbf{o}$ ). In the conventional notation of the conformal MOG, the basis vectors of the representational space are:

$$\{\mathbf{o}, \mathbf{e}_1, \mathbf{e}_2, \cdots, \mathbf{e}_d, \mathbf{\infty}\},$$
 (C.1)

where  $\{\mathbf{e}_i\}_{i=1}^d$  define the Euclidean, and  $\{\mathbf{o}, \infty\}$  define the non-Euclidean portions of the total space (see the multiplication table for the vector inner product of the basis vectors under conformal MOG in Supplementary Material A).

In order to have an accumulator array that approximates the Voronoi diagram, one has to assume the following order for the basis vectors of the representational space:

$$\{\mathbf{e}_1, \mathbf{e}_2, \cdots, \mathbf{e}_d, \mathbf{\infty}, \mathbf{o}\}$$
. (C.2)

Such an ordering of basis vectors is important for retrieving the Voronoi diagram because it gives the appropriate geometric interpretation to the parameters of our parameterization scheme. The study of the interpretation of parameters regarding all possible ordering of basis vectors is out of the scope of this work. We have used the conventional ordering of basis vectors in other (d-1)-spheres detection examples presented in our manuscript [2].

After defining the basis vector as (C.2), one has to replace the actual degenerate metric of the representational space by a more convenient metric while performing the proposed subspace detection scheme (as discussed in our paper [2] – Section 4.1). By assuming Euclidean metric for  $\mathbb{R}^n$ , the basis vectors in (C.2) map to the basis vectors of some Euclidean space, *i.e.*,

$$egin{aligned} \mathbf{e}_1 &\mapsto \mathbf{e}_1, \ \mathbf{e}_2 &\mapsto \mathbf{e}_2, \ & \vdots \ \mathbf{e}_d &\mapsto \mathbf{e}_{n-2}, \ \mathbf{o} &\mapsto \mathbf{e}_{n-1}, \ \mathbf{\infty} &\mapsto \mathbf{e}_n, \end{aligned}$$

leading to the following (Euclidean) vector basis:

$$\{\mathbf{e}_1, \mathbf{e}_2, \cdots, \mathbf{e}_n\}$$
. (C.3)

Recall that the intended subspaces are geometric interpreted as (d-1)-spheres under the conformal MOG. The dimensionality of such subspaces is p = n - 1. As a result, the proposed model function for p-blades (i.e., equation (15) in our paper [2]):

$$\mathbf{B}_{\langle p \rangle} = \mathbf{T} \, \mathbf{E}_{\langle p \rangle} \, \widetilde{\mathbf{T}}, \tag{C.4}$$

reduces to

$$\mathbf{B}_{\langle n-1\rangle} = \mathbf{S}_n \, \mathbf{E}_{\langle n-1\rangle} \, \widetilde{\mathbf{S}}_n \tag{C.5}$$

by replacing the rotor T in (C.4) by its component rotor

$$S_n = R_{n,1} \cdots R_{n,n-2} R_{n,n-1},$$
 (C.6)

where rotors  $R_{n,j}$  are defined as:

$$\mathbf{R}_{n,j} = \cos\left(\frac{\theta^{n,j}}{2}\right) - \sin\left(\frac{\theta^{n,j}}{2}\right) \left(\mathbf{e}_{j+1} \wedge \mathbf{e}_{j}\right), \tag{C.7}$$

for  $j \in \{n-1, n-2, \dots, 1\}$  (see (23), (18) and (19) in [2]). The rotation angles  $\theta^{n,j}$  related to  $\mathbf{R}_{n,j}$  in (C.7) are the parameters characterizing the attitude of p-blades, and hence the intended (d-1)-spheres.

The blade  $\mathbf{E}_{\langle n-1\rangle}$  in (C.5) is a canonical subspace used as reference (see (21) in the paper). It is defined as

$$\mathbf{E}_{\langle n-1\rangle} = \mathbf{e}_n^*$$

$$= (-1)^{d(d+1)/2} \mathbf{e}_1 \wedge \mathbf{e}_2 \wedge \dots \wedge \mathbf{e}_{n-1}.$$
(C.8)

Under the assumed Euclidean metric,  $\mathbf{E}_{\langle n-1\rangle}$  is just a (n-1)-dimensional Euclidean subspace. However, under the actual conformal MOG, the blade  $\mathbf{E}_{\langle n-1\rangle}$  is written as

$$\mathbf{E}_{\langle n-1\rangle} = (-1)^{d(d+1)/2} \, \mathbf{e}_1 \wedge \mathbf{e}_2 \wedge \cdots \wedge \mathbf{e}_d \wedge \mathbf{\infty},$$

and it is geometrically interpreted as an improper (d-1)-flat. In practice, it means that the reference blade  $\mathbf{E}_{\langle n-1\rangle}$  is a straight line at infinity when a 2-dimensional base space is assumed (d=2), or a plane at infinity by assuming some 3-dimensional base space (d=3), and so on.

# C.3 Geometric Interpretation of the Parameters

According to (C.5), (C.6), and (C.7), the proposed subspace detection scheme defines a sequence of (n-1) rotation operations applied to blade  $\mathbf{E}_{(n-1)}$  (C.8) under the assumed Euclidean MOG. The first rotation is encoded by rotor  $\mathbf{R}_{n,n-1}$ . Under the conformal MOG, the resulting blade may be interpreted as

some real or imaginary (d-1)-sphere at the origin of the base space, with square radius  $(r_{origin}^2)$  varying in the  $(-\infty, +\infty)$  range in function of the value of  $\theta^{n,n-1}$  (i.e., the rotation angle in  $\mathbf{R}_{n,n-1}$ ). The relation between  $r_{origin}$  and  $\theta^{n,n-1}$  is given by:

$$r_{origin} = \sqrt{2 \tan\left(\theta^{n,n-1} + \frac{\pi}{2}\right)},$$
 (C.9)

where  $r_{origin}$  is real for  $\theta^{n,n-1} \in [-\pi/2,0)$ , and imaginary for  $\theta^{n,n-1} \in (0,\pi/2)$ . When  $\theta^{n,n-1} = 0$ , the resulting blade is  $\mathbf{E}_{\langle n-1 \rangle}$  without change.

The second transformation performed in (C.5) is encoded by  $\mathbf{R}_{n,n-2}$ . It is applied to blade  $\mathbf{R}_{n,n-1} \mathbf{E}_{\langle n-1 \rangle} \tilde{\mathbf{R}}_{n,n-1}$ . Under the conformal MOG, such a transformation may be interpreted as scaling a (d-1)-sphere at the origin of the base space by some factor  $\alpha \geq 1$ , followed by translating the scaled (d-1)-sphere along the line through the origin  $\mathbf{o}$  with direction  $\mathbf{e}_d$ . The radius r of the resulting (d-1)-sphere and the distance t of its center from the origin of the base space are given, respectively, by:

$$r = \sqrt{\frac{r_{origin}^2}{\cos(\theta^{n,n-2})} + \tan^2(\theta^{n,n-2})},$$
 (C.10)

and

$$t = -\tan\left(\theta^{n,n-2}\right),\tag{C.11}$$

where  $r_{origin}$  is defined in (C.9), and  $\theta^{n,n-2}$  is the rotation angle related to the rotor  $\mathbf{R}_{n,n-2}$ .

The other rotors applied to  $\mathbf{E}_{\langle n-1\rangle}$  in (C.5) (i.e.,  $\mathbf{R}_{n,i}$ , for  $i \in \{n-3, n-4, \cdots, 1\}$ ) encode rotation operations on planes defined by the basis vectors of the Euclidean base space  $\mathbb{R}^d$ . As a result, under the conformal MOG those transformations are geometrically interpreted as rotating the (d-1)-sphere  $\mathbf{R}_{n,n-2} \mathbf{R}_{n,n-1} \mathbf{E}_{\langle n-1\rangle} \tilde{\mathbf{R}}_{n,n-1} \tilde{\mathbf{R}}_{n,n-2}$  around the origin of  $\mathbb{R}^d$ . Therefore, the geometric interpretation of the transformations in  $\mathbf{R}_{n,i}$  makes  $\theta^{n,i}$  equivalent to the rotational portion of a hyperspherical coordinate system [3].

#### C.3.1 The Standard Hough Transform

The standard HT for circle detection in the plane is usually defined regarding the center-radius parameterization of the circle. For instance, the circle detection proposed by Duda and Hart [4] uses

$$(x - x_c)^2 + (y - y_c)^2 - r^2 = 0$$
 (C.12)

as model function, while Kimme et al. [5] assume

$$\begin{bmatrix} x \\ y \end{bmatrix} = \begin{bmatrix} x_c \\ y_c \end{bmatrix} + r \begin{bmatrix} \cos(\phi_t) \\ \sin(\phi_t) \end{bmatrix}$$
 (C.13)

as model for circles. In (C.12) and (C.13),  $(x_c, y_c, r)$  is the parameter vector for circles centered at  $(x_c, y_c)$  and with radius r. Both models expect point coordinates (x, y) as input.

When applied to the same detection case, the parameter vector of our subspace detection scheme is  $\{\theta^{4,3}, \theta^{4,2}, \theta^{4,1}\}$ . The relation between the r parameter of standard HTs for circles in the plane and the proposed parameters is given by (C.10). It is important to comment that by restricting input point coordinates to the  $[-1,1] \times [-1,1]$  range, the contribution of  $\theta^{4,2}$  to the circle's radius is proportionally (much) smaller than the contribution of  $\theta^{4,3}$ . Such a contribution is computed as  $r/r_{origin}$ , where  $r_{origin}$  (C.9) is fully determined by  $\theta^{4,3}$ . Therefore, one can assume that the value of r is encoded by  $\theta^{4,3}$ . The relation between the  $(x_c, y_c)$  parameters of standard HTs and the proposed parameterization is given by replacing the conventional Cartesian coordinate system by a polar coordinate system, where  $\theta^{4,2}$  encodes the displacement of circles from the origin of the image space, and  $\theta^{4,1}$  the rotation of displaced circles on the image plane.

In contrast to standard HTs for circle detection, our approach naturally extends to the concurrent detection of straight lines. It is possible because 3-blades under the conformal MOG can be geometrically interpreted as circles or as straight lines (see Supplementary Material A, Section A.4). In such a case, one can think on a straight line as a circle with infinity radius whose (straight) circumference crosses the image plane. The set of parameter vectors representing all possible straight lines reside in the  $\{\theta^{4,3}, \theta^{4,1}\}$ -plane of the parameter space where  $\theta^{4,2} = -\pi/2$ .

Notice that pairs of points (as a single element), free directions, and tangent direction are not accepted as input entries of the model functions used by Duda and Hart [4] and Kimme *et al.* [5]. Our approach, on the other hand, is independent of the type of input data.

#### C.4 Retrieving the Voronoi Diagram

Fig. C.1b presents an approximation of the 2th-order Voronoi diagram in  $\mathbb{R}^2$  (thus, n=2+2=4) retrieved by using our subspace detection framework in the points depicted in Fig. C.1a. These points were encoded in conformal

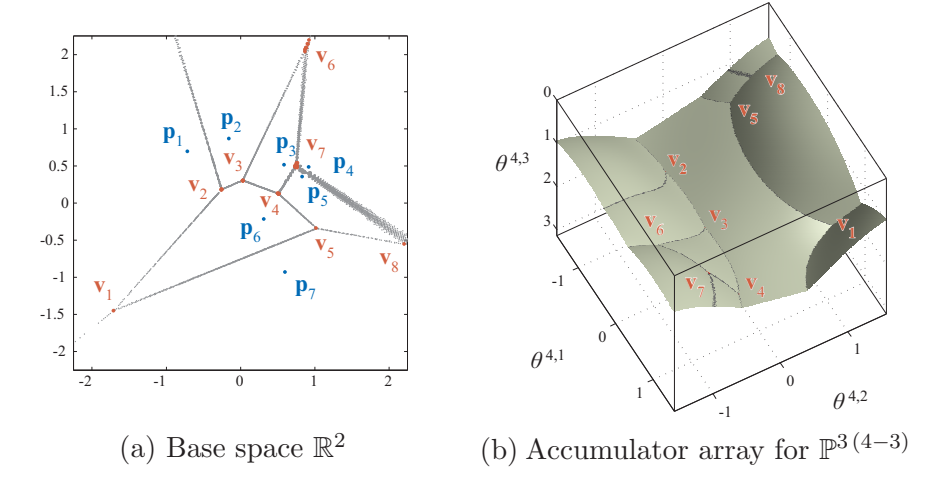


Fig. C.1. The Voronoi diagram of a set of points can be retrieved from the accumulator array produced while performing circle detection with the conformal MOG: (a) The vertices ( $\mathbf{v}_j$ ) and edges (approximated by gray points) of the Voronoi diagram of points  $\mathbf{p}_i$  are defined by the center of circles having no points in their interior and passing through more than two, and passing through exactly two input points, respectively. (b) These circles reside on a well defined surface at the parameter space. They can be identified as the bins, in such surface, having more than two and two votes, respectively. The multiple detection of vertices  $\mathbf{v}_6$ ,  $\mathbf{v}_7$  and  $\mathbf{v}_8$  in (a), and the width of the edge between  $\mathbf{p}_4$  and  $\mathbf{p}_5$  are related to the quasi-alignment of the surfaces related to  $\mathbf{p}_4$  and  $\mathbf{p}_5$  in parameter space, leading to multiple intersections while defining the surface depicted in (b).

MOG as 1-blades:

$$\mathbf{p}_k = x_k \, \mathbf{e}_1 + y_k \, \mathbf{e}_2 + \frac{x_k^2 + y_k^2}{2} \, \mathbf{\infty} + 1 \, \mathbf{o},$$
 (C.14)

and used as input for the detection of circles (p = 3). In (C.14),  $(x_k, y_k)$  are the coordinates of the k-th point, and  $\{\mathbf{e}_1, \mathbf{e}_2, \mathbf{\infty}, \mathbf{o}\}$  are basis vectors of the representational space, as explained in Section C.2.

While performing the voting procedure for subspace detection, each input blade/point  $\mathbf{p}$  maps to a surface in the 3-dimensional parameter space (thus, m=3 (4-3) = 3 in this example). The voting procedure increments the bins of the accumulator array related to such a mapping. From the intersection of p=3 or more surfaces one retrieves the circles passing thought three or more input points. Recall that the center of the circles having the smaller radius corresponds to the vertices of the Voronoi diagram (points  $\mathbf{v}_j$  in Fig. C.1a). Therefore, by finding the bins corresponding to the circles having the smaller radius and receiving three or more votes, one finds the vertices of the Voronoi diagram.

The parts of the surfaces closest to the origin of the parameter space and at the positive side of the  $\theta^1$ -axis (or  $\theta^{3,2}$  in double-index notation) are comprised by

the parameter vector of the circles with smaller square radius. This relation between  $\theta^{3,2}$  and the square radius of circles can be derived from (C.9) by computing  $r_{origin}^2$ , and by mapping  $\theta^{3,2}$  to the  $[0, \pi/2)$  range. Notice that the square of  $r_{origin}$  for imaginary circles is negative, while for conventional circles is zero or positive. As Fig. C.1b shows, the circles with smaller radius reside (in parameter space) on a surface defined by the superposition of mapped input data. Thus, the vertices of the diagram can be retrieve just by looking for the bins having the largest values on that surface (i.e., more than d=2 votes). The bins having d votes correspond to the circles whose centers are at an edge of the Voronoi diagram (the gray points in Fig. C.1a).

The votes accumulated by the bins behind the green surface in Fig. C.1b are not shown for sake of clarity. It is important to emphasize that, by definition, no vote is cast in front of the green surface. In this example, the discretization step for defining the accumulator array is  $\pi/720$ , and  $\omega=1$ . The extension of the example describe in this section to higher-dimensions is straightforward.

#### C.5 Related Work

The idea of using a rasterizing scheme to construct 2-dimensional Voronoi diagrams of points was first suggested by Haeberli [6], and efficiently implemented in Graphics Hardware by Hoff et al. [7]. The approach computes the discrete diagram by Z-buffering right circular cones onto a 2-dimensional canvas. The base of the cones is defined as being parallel to the image plane and the apex points are located at the point sites. By rendering a polygonal approximation of the cones, all distances across the polygonal mesh are represented and stored as depth in a Z-buffer. The Z-buffer depth test compares the new depth value to the previously stored value. If the new value is less, the Z-buffer records the new distance, and the frame buffer records the site's ID as a unique color assigned to each site. In this way, each pixel in the frame buffer will have a color corresponding to its closest site, and the depth-buffer will have the distance to that site. After all the cones have being rendered, an approximation of the Voronoi diagram can be retrieved from the boundaries of the resulting image.

#### References

 G. Voronoi, Nouvelles applications des paramètres continus à la théorie des formes quadratiques, J. Reine Angew. Math. (Crelle's J.) 1908 (134) (1908) 198– 287.

- [2] L. A. F. Fernandes, M. M. Oliveira, A general framework for subspace detection in unordered multidimensional data, Pattern Recognit.(submitted).
- [3] A. Erdélyi (Ed.), Higher transcendental functions, Vol. 2, McGraw Hill, 1981.
- [4] R. O. Duda, P. E. Hart, Use of the Hough transformation to detect lines and curves in pictures, Commun. ACM 15 (1) (1972) 11–15.
- [5] C. Kimme, D. Ballard, J. Sklansky, Finding circles by an array of accumulators, Commun. ACM 18 (2) (1975) 120–122.
- [6] P. Haeberli, Paint by numbers: abstract image representations, in: Proc. of ACM SIGGRAPH, 1990, pp. 207–214.
- [7] K. E. Hoff, J. Keyser, M. Lin, D. Manocha, T. Culver, Fast computation of generalized Voronoi diagrams using graphics hardware, in: Proc. of ACM SIGGRAPH, 1999, pp. 277–286.